Supplementary Information for

Formation of Phosphine Imide ($HN=PH_3$) and its Phosphinous Amide ($H_2N–PH_2$) Isomer

Cheng Zhu,[a,b] Alexandre Bergantini,[a,b§] Santosh K. Singh,[a,b] Ralf I. Kaiser[a,b*]

[a]*Department of Chemistry, University of Hawaii at Manoa, 2545 McCarthy Mall, Honolulu, HI 96822 (USA)*

[b]*W. M. Keck Laboratory in Astrochemistry, University of Hawaii at Manoa, 2545 McCarthy Mall, Honolulu, HI 96822 (USA)*

André K. Eckhardt,[c#*] Peter R. Schreiner[c]

[c]*Institute of Organic Chemistry, Justus Liebig University, Heinrich-Buff-Ring 17, 35392 Giessen (Germany)*

Ya-Syuan Huang,[d] Bing-Jian Sun,[d] Agnes H. H. Chang[d*]

[d]*Department of Chemistry, National Dong Hwa University, Shoufeng, Hualien 974, Taiwan*

[§]Present address: *Centro Federal de Educacao Tecnologica Celso Suckow da Fonseca - CEFET/RJ, Av. Maracana 229, 20271-110, Rio de Janeiro, (Brazil)*

[#]Present address: *MIT Department of Chemistry, Cambridge, MA 02139 (USA)*

*Correspondence to: hhchang@gms.ndhu.edu.tw, ake05@mit.edu, ralfk@hawaii.edu

Materials and Methods – Experimental

The experiments were performed at the W. M. Keck Research Laboratory in Astrochemistry.[1] The experimental setup consists of a contamination-free stainless steel ultra-high vacuum chamber (UHV) evacuated to a base pressure of a few 10^{-11} Torr by magnetically levitated turbo molecular pumps coupled to oil-free scroll backing pumps. Within the chamber, a silver mirror substrate is interfaced to a cold finger, which is connected to a closed cycle helium compressor (Sumitomo Heavy Industries, RDK-415E). By utilizing a doubly differentially pumped rotational feedthrough (Thermionics Vacuum Products, RNN-600/FA/ MCO) and an UHV compatible bellow (McAllister, BLT106), the substrate is able to be rotated in the horizontal plane and to be translated vertically, respectively. The temperature of the silver wafer was monitored by a silicon diode sensor (Lakeshore DT-470) and regulated in a range of 5 to 300 K with a precision of ± 0.1 K by a programmable temperature controller (Lakeshore 336). After the wafer reached 5.0 ± 0.1 K, phosphine (PH_3, Sigma-Aldrich, 99.9995 %) and ammonia (NH_3, Matheson, 99.9992%) (Table S1) were co-deposited onto it via two glass capillary arrays. During the deposition, the total pressure of PH_3 and NH_3 in the main chamber was maintained at $(2.0 \pm 0.2) \times 10^{-8}$ torr with $(1.0 \pm 0.1) \times 10^{-8}$ torr for each species for about 32 minutes. Isotopically labeled ^{15}N-ammonia ($^{15}NH_3$, Sigma-Aldrich, 98% ^{15}N) and heavy ammonia (ND_3, Sigma-Aldrich, 99% D) were utilized in duplicate experiments to observe infrared absorption and mass shifts of products. The overall thickness of the ice was determined using laser interferometry[2] with one helium-neon laser (CVI Melles Griot; 25-LHP-230) operating at 632.8 nm. The laser light was reflected at an angle of 2° relative to the ice surface normal. Considering the refractive indexes of pure ices $n_{PH_3} = 1.51 \pm 0.04$ and $n_{NH_3} = 1.41 \pm 0.04$,[3-6] the ice thickness was calculated to be 1410 ± 50 nm.

Mid-infrared (6,000 to 400 cm^{-1}) spectra of the ices were recorded utilizing a Nicolet 6700 Fourier transform infrared (FTIR) spectrometer with 4 cm^{-1} spectral resolution. The FTIR spectra of the pristine ice is shown in Fig. S1. Detailed assignments of the peaks are compiled in Table S2.[3, 7–11] The ice composition was determined via a modified Beer-Lambert law.[12] Peak areas are not guaranteed to be linear to ice thickness due to optical interference;[13] however, this problem can be circumvented by selecting only weak bands.[14] For PH_3, the average column density was determined to be $(1.9 \pm 0.5) \times 10^{18}$ molecules cm^{-2} based on the integrated areas along with absorption coefficient of 5.1×10^{-19} cm $molecule^{-1}$ for 985 cm^{-1} (ν_2) band.[3] The

average column density of NH_3 was calculated to be $(1.3 \pm 0.4) \times 10^{18}$ molecules cm^{-2} based on the integrated areas along with absorption coefficient of 5.6×10^{-18} cm $molecule^{-1}$ for 1625 cm^{-1} (ν_4) band.[15, 16] Therefore, the ratio of PH_3 and NH_3 was found to be $(1.6 \pm 0.5) : 1$.

The ices were then isothermally irradiated at 5.0 ± 0.1 K with 5 keV electrons (Specs EQ 22-35 electron source) at a 70° angle to the ice surface normal for 15 min at currents of 0 nA (blank) and 20 nA (Table S1). Using Monte Carlo simulations (CASINO 2.42),[17] the average and maximum penetration depths of the electrons were calculated to be 360 ± 40 nm and 830 ± 90 nm, respectively (Table S3), which are less than the 1080 ± 50 nm ice thickness ensuring no interaction between the impinging electrons and the silver substrate. With the parameters compiled in Table S3, the irradiation doses at 20 nA were calculated to be 0.8 ± 0.2 eV per PH_3 molecule and 0.4 ± 0.1 eV per NH_3 molecule. During the irradiation, in situ mid-infrared spectra of the ices were recorded every 2 minutes.

After the irradiation, the ices were heated to 300 K at a rate of 1 K min^{-1} (temperature programmed desorption (TPD)). During the TPD phase, any subliming molecules were detected using a reflectron time-of-flight (ReTOF) mass spectrometer (Jordon TOF Products, Inc.) with single photon ionization[1] (Figs. 3 and 4, Figs. S2 - S4, Table S4 and S5). This photoionization process utilizes difference four wave mixing to produce vacuum ultraviolet light ($\omega_{vuv} = 2\omega_1 - \omega_2$) (Table S4). The experiments were performed with 10.49 eV, 9.43 eV, 8.80 eV, and 8.20 eV photoionization energies to distinguish between the PNH_4 isomers. The 10.49 eV (118.222 nm) light was generated via frequency tripling ($\omega_{vuv} = 3\omega_1$) of the third harmonic (355 nm) of the fundamental of a Nd:YAG laser (YAG A) in pulsed gas jets of Xe. To produce 9.43 eV, the third harmonic (355 nm) of a Nd:YAG laser was used to pump a Coumarin 450 dye (0.20 g L^{-1} ethanol) to obtain 445.132 nm (2.72 eV) (Sirah, Cobra-Stretch), which underwent a frequency doubling process to achieve ω_1 = 222.566 nm (5.57 eV) (β-BaB_2O_4 (BBO) crystals, 57.4°). A second Nd:YAG laser (second harmonic at 532 nm) pumped LDS 722 dye (0.25 g L^{-1} ethanol) to obtain ω_2 = 725 nm (1.72 eV), which then combined with $2\omega_1$, using Xenon as a non-linear medium, generated ω_{vuv} = 136.462 nm (9.43 eV) at 10^{12} photons per pulse. The settings for generating 140.860 nm (8.80 eV) light is the same as that for 136.462 nm (9.43 eV) except substitution of the LDS 722 dye by Coumarin 540A dye (1.60 g L^{-1} ethanol) to produce 530 nm

(2.34 eV) light. The settings for generating 151.200 nm (8.20 eV) light is also the same as that for 136.462 nm (9.43 eV) except substitution of the Coumarin 450 dye by Coumarin 503 dye (0.40 g L^{-1} ethanol) to produce 499.256 nm (2.48 eV) light and using the LDS 722 dye to generate 715 nm (1.73 eV) light. The VUV light was spatially separated from other wavelengths (due to multiple resonant and non-resonant processes ($2\omega_1 + \omega_2$; $3\omega_1$; $3\omega_2$)) using a lithium fluoride (LiF) biconvex lens (ISP Optics) and directed 2 mm above the sample to ionize subliming molecules. The ionized molecules were mass analyzed with the ReTOF mass spectrometer where the arrival time to a multichannel plate is based on mass-to-charge ratios, and the signal was amplified with a fast preamplifier (Ortec 9305) and recorded with a personal computer multichannel scalar (FAST ComTec, P7888-1 E), which is triggered via a pulse delay generator at 30 Hz. Here the ReTOF signal is the average of 3600 sweeps of the mass spectrum in 4 ns bin widths, which corresponds to an increase of the substrate temperature of 2 K.

Materials and Methods – Theoretical

All computations were carried out with Gaussian 09, Revision D.01 and Gaussian 16, Revision A.03 (Fig. S5 - S6, Tables S6 - S11).[18, 19] For geometry optimizations and frequency computations, the density functional theory (DFT) B3LYP functional[20-22] was employed utilizing the Dunning correlation consistent split valence basis set cc-pVTZ.[23] Based on these geometries, the corresponding coupled cluster[24-27] CCSD(T)/cc-pVDZ, CCSD(T)/cc-pVTZ, and CCSD(T)/cc-pVQZ single point energies were computed and extrapolated to complete basis set limit[28] CCSD(T)/CBS with B3LYP/cc-pVTZ zero-point vibrational energy (ZPVE) corrections. The adiabatic ionization energies were computed by taking the ZPVE corrected energy difference between the neutral and ionic species that correspond to similar conformations. To determine the quality of the single-reference-based electron correlation methods, we performed T1 diagnostics. The T1 values for phosphine imide ($HN{=}PH_3$, 1), phosphinous amide ($H_2N{-}PH_2$, 4), and phosphinoammonium ($H_3N{=}PH$, 5) were computed to be 0.014, 0.011, and 0.0106, respectively, which are less than 0.02, thus confirming that the single-reference-based electron correlation methods ought to be reliable according to recommendations in the current literature.[29] The ionization energies were corrected for the Stark effect by 0.03 eV.[30] Natural bond orbitals were computed with the NBO6 program.[31]

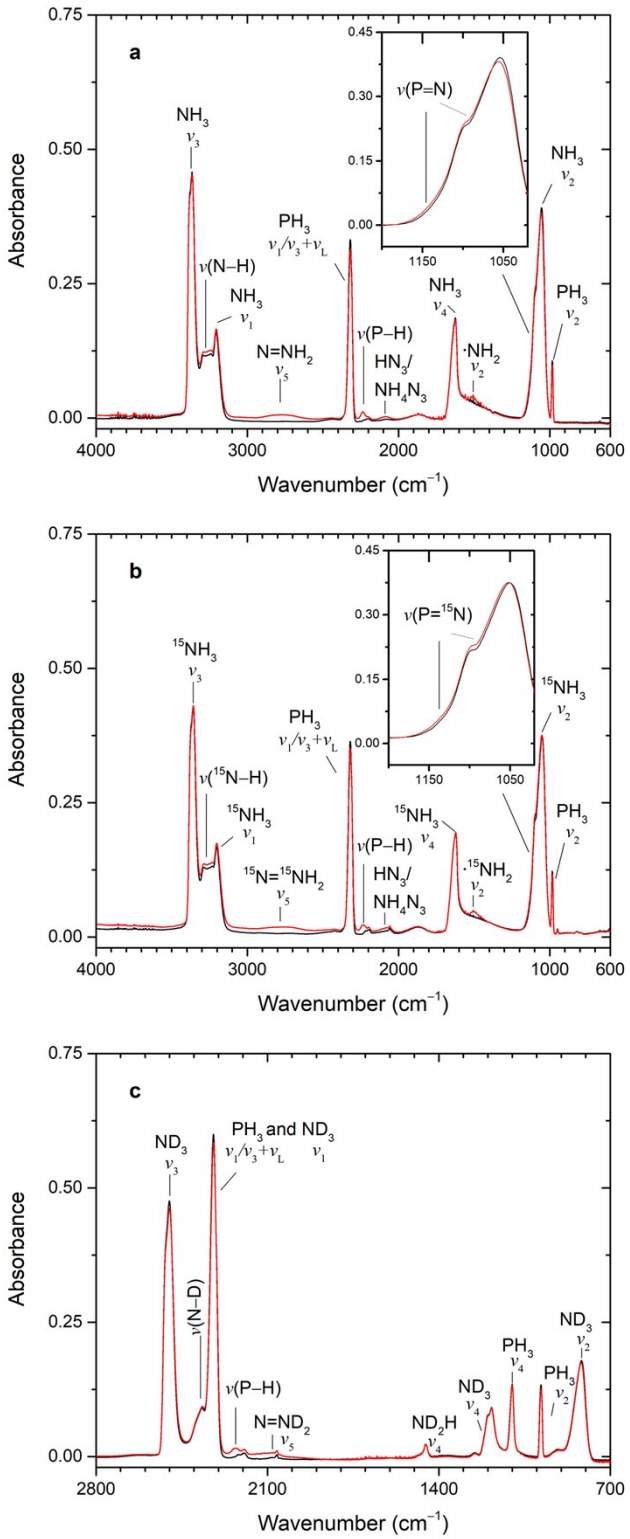

Fig. S1 FTIR spectra of the phosphine (PH_3) + ammonia (NH_3) (a), phosphine (PH_3) + ^{15}N-ammonia ($^{15}NH_3$) (b), and phosphine (PH_3) + D-ammonia (ND_3) (c) ices before (black) and after (red) processing with energetic electrons.

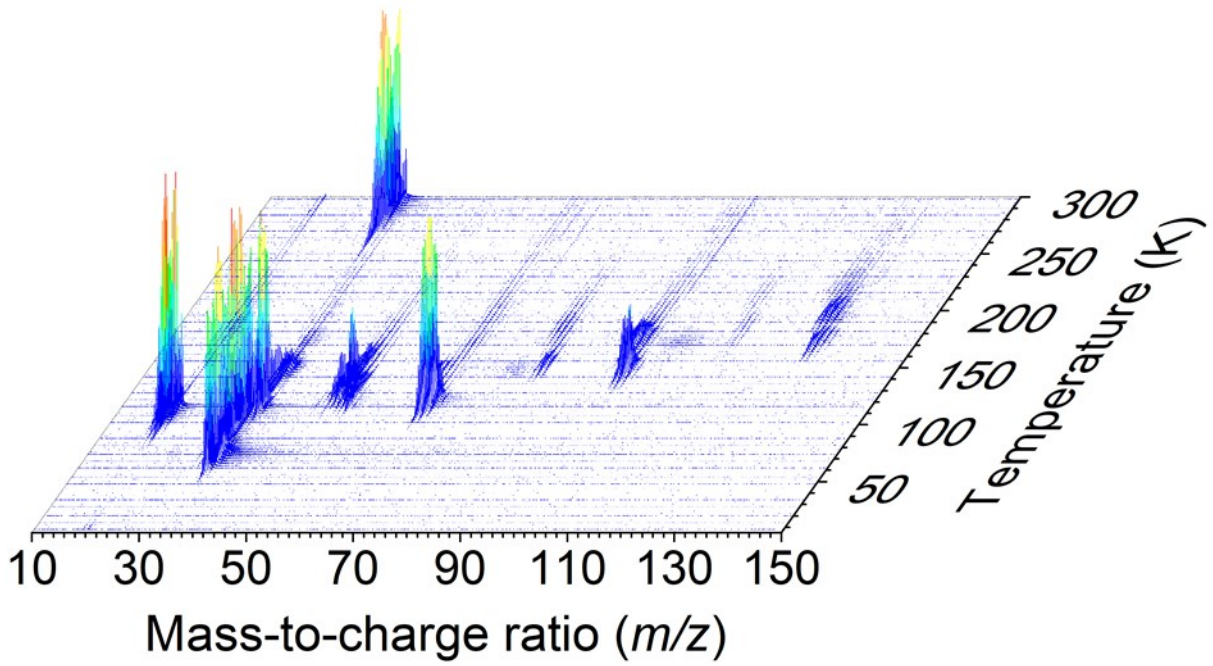

Fig. S2 PI-ReTOF-MS data during the temperature programmed desorption (TPD) phase of the electron processed phosphine (PH_3) + heavy ammonia (ND_3) ice (PI = 10.49 eV).

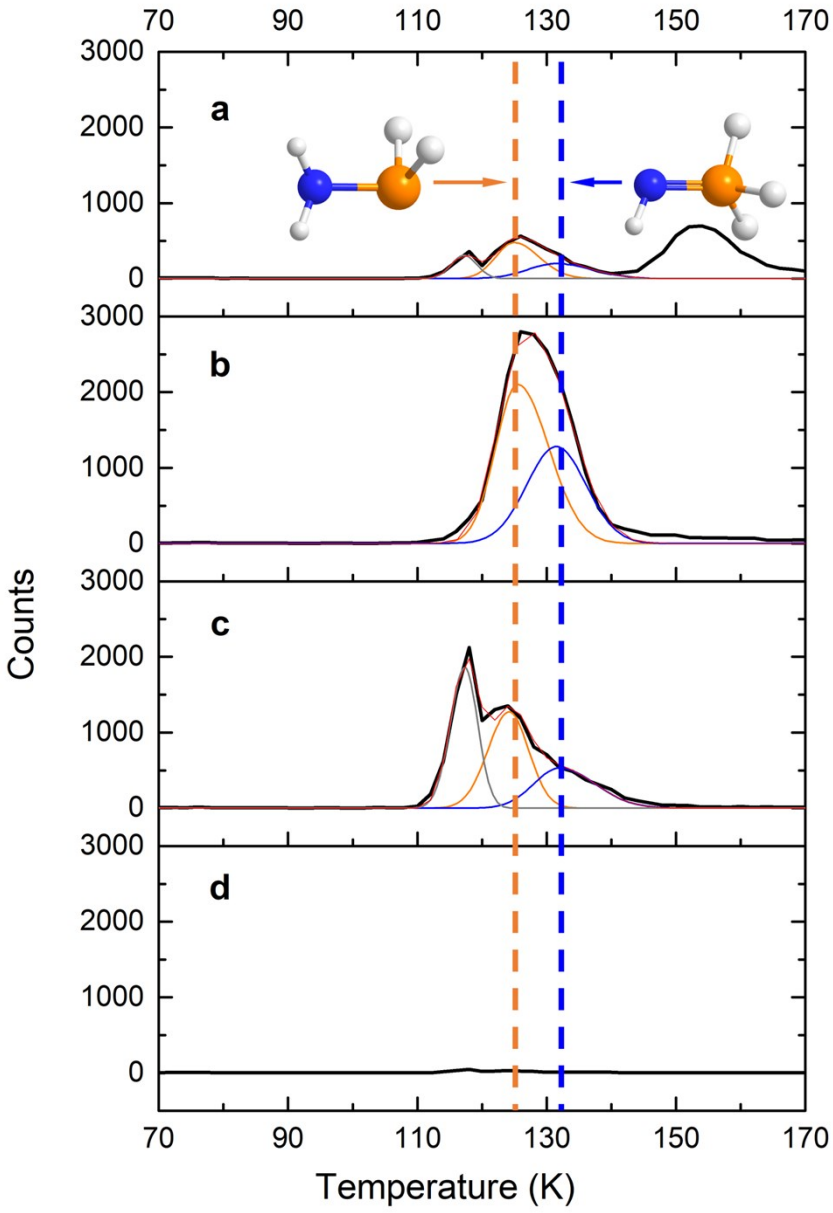

Fig. S3 PI-ReTOF-MS data during the temperature programmed desorption (TPD) phase of the electron processed phosphine (PH_3) + heavy ammonia (ND_3) ice (PI = 10.49 eV). **a**, *m/z* = 50, NPH_3D^+. **b**, *m/z* = 51, $NPH_2D_2^+$. **c**, *m/z* = 52, $NPHD_3^+$. **d**, *m/z* = 53, NPD_4^+.The carriers of the peaks at 118 K and 153 K in **a** and 118 K in **c** are tentatively linked to $NPHD_2^+$, $NPHD_2^+$, and $NPH_3D_2^+$ fragments of $N_2PH_3D_2^+/N_2PH_2D_3^+/N_2PHD_5^+$, $NP_2H_4D^+/NP_2H_3D_2^+/NP_2H_2D_3^+$, and $N_2PH_3D_2^+$, respectively.

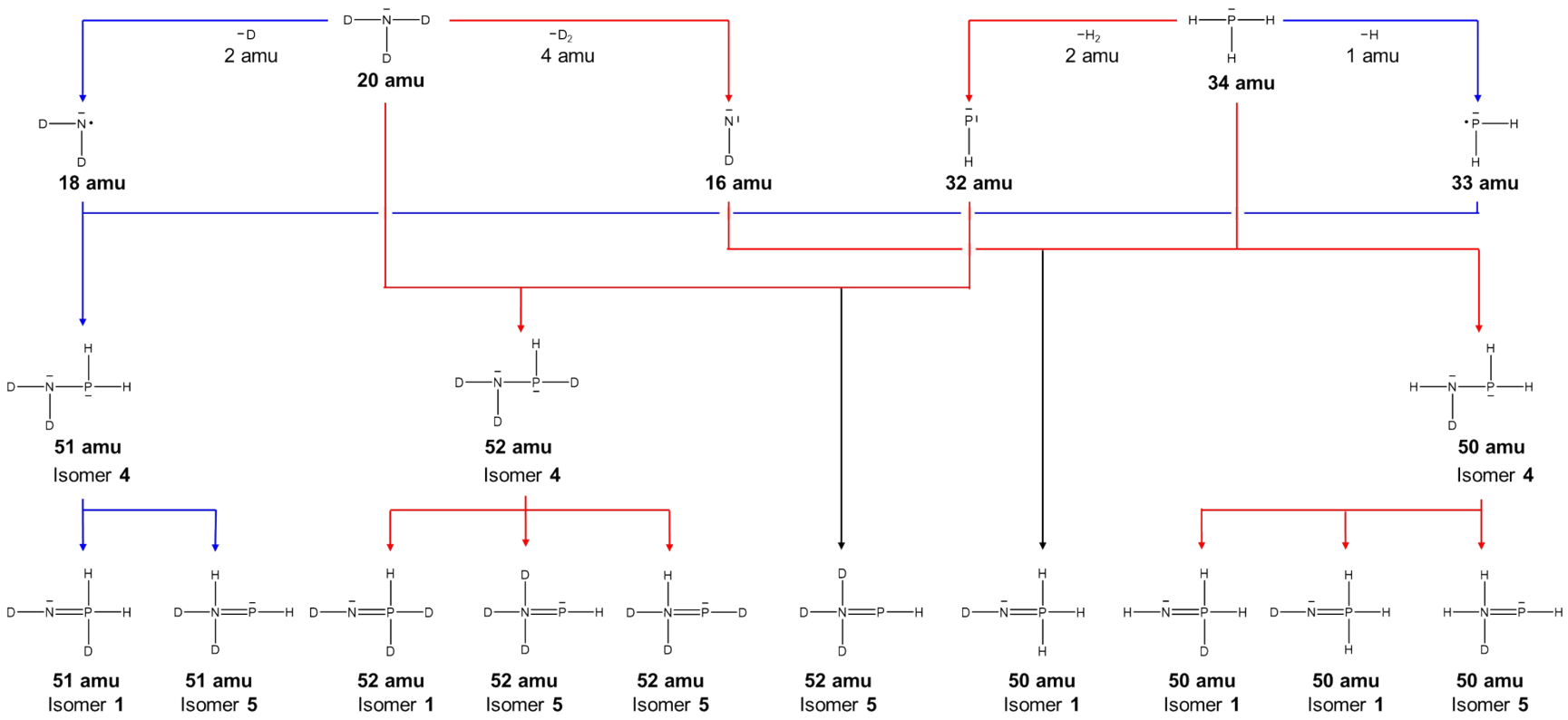

Fig. S4 Schematic representation of the formation of partially deuterated **1**, **4**, and **5** isomers from phosphine (PH_3) and heavy ammonia (ND_3). Radical-radical, insertion, and addition pathways are color coded in blue, red, and black, respectively.

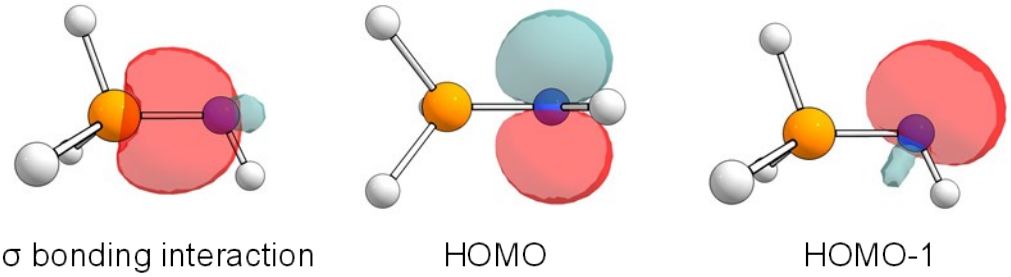

Fig. S5 Bond characters of phosphine imide ($HN=PH_3$, **1**).

We explored the bond characters of phosphine imide (**1**). The PN bond length of **1** (1.57 Å) is shorter than a P–N single bond (e.g., 1.77 Å in the anion of the salt $Na^+[H_3NPO_3]^-$) and is close to that of P=N double bonds of phosphazenes (1.56 Å in hexafluorocyclotriphosphazene $(NPF_2)_3$ and 1.60 Å in hexachlorocyclotriphosphazene $(NPCl_2)_3$).[32] However, natural resonance theory (NRT) analysis found that the Wiberg index of the PN bond is 1.34 and that the zwitterionic contributor is the leading resonance structure (50%). The neutral PN double bond structure only has a minor contribution (< 1%). Furthermore, there is no π bonding orbital interaction but only σ bonding interaction between the nitrogen and phosphorus atoms (Fig. S4). These results indicate that **1** is best described as a zwitterion. The highest occupied molecular orbital (HOMO) and HOMO – 1 are located on the nitrogen atom and represent lone pair electrons and negative charges in *p*- and σ_{out}-type non-bonding orbitals (Fig. S4). This is in line with a previous computational investigation of the H_3PNH plus formaldehyde (H_2CO) reaction,[33] which starts with the attack of the nitrogen atom of the nucleophile (H_3PNH) on the electrophilic formaldehyde carbon.

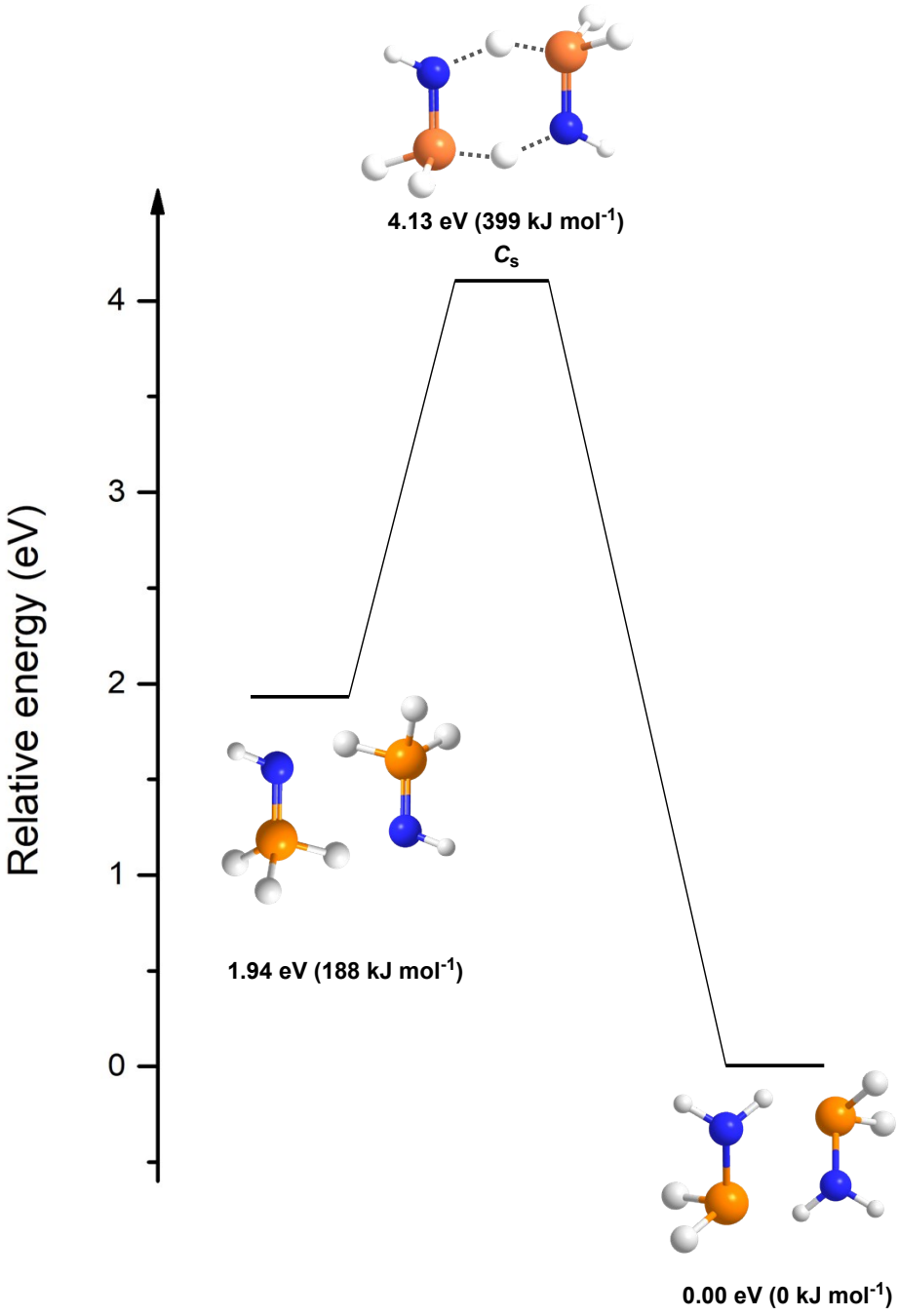

Fig. S6 Potential energy surface for intermolecular H-transfer between two phosphine imide ($HNPH_3$, **1**) molecules at CCSD(T)/CBS//B3LYP/cc-pVTZ including zero-point vibrational energy (ZPVE). The atoms are color coded in white (hydrogen), blue (nitrogen), and orange (phosphorous). The barrier of 211 kJ mol^{-1} is slightly lower than the unimolecular isomerization barrier from **1** to **4** (214 kJ mol^{-1}). These high barriers suggest that isomer **1** is stable once generated.

Table S1. List of experiments.

#	Precursors	Electron current (nA)	Irradiation time (min)	Photoionization Energy (eV)
1	$PH_3 + NH_3$	0 (blank)	-	10.49
2	$PH_3 + NH_3$	20	15	10.49
3	$PH_3 + {}^{15}NH_3$	20	15	10.49
4	$PH_3 + ND_3$	20	15	10.49
5	$PH_3 + NH_3$	20	15	9.43
6	$PH_3 + NH_3$	20	15	8.80
7	$PH_3 + NH_3$	20	15	8.20

Table S2. Infrared absorption peaks before and after irradiation for phosphine (PH_3) + ammonia (NH_3) / ^{15}N-ammonia ($^{15}NH_3$) / D-ammonia (ND_3) ices[a].

Pristine ice, before irradiation (5 K)			
Assignment	Position with NH_3 (cm^{-1})	Position with $^{15}NH_3$ (cm^{-1})	Position with ND_3 (cm^{-1})
PH_3 (v_2)	985	985	984
NH_3 (v_2)	1057	1051	820
PH_3 (v_4)	1100	1100	1101
NH_3 (v_4)	1627	1623	1185
PH_3 ($2v_4$)	2199	2199	2198
PH_3 (v_1/v_3)	2321	2321	2321
PH_3 ($v_1/v_3 + v_L$)	2432	2431	Overlap with ND_3
NH_3 (v_1)	3212	3205	Overlap with PH_3
NH_3 (v_3)	3369, 3386	3360, 3377	2500
New peaks after irradiation (5 K)			
$v_{(P–N)}$	1100, 1154	1094, 1140	Overlap with ND_3
$•NH_2$ (v_2)	1508	1503	Overlap with ND_3
HN_3 and/or NH_4N_3	2090	2080	Overlap with $N=ND_2$
$v_{P–H}$	2238	2238	2236
$N=NH_2$ (v_5)	2785	2776	2085
$v_{N–H}$	3365, 3330	3160, 3320	2370

Note.

[a] References: Shimanouchi (1977), Teles et al. (1989), Socrates (2004), Holt et al. (2004), Zheng et al. (2008), Turner et al. (2015).

Table S3. Data applied to calculate the average irradiation dose per molecule.

Initial kinetic energy of the electrons, E_{init} (keV)		5
Ice		$PH_3 + NH_3$
Irradiation current, I (nA)		20 ± 1
Total number of electrons		$(1.1 \pm 0.1) \times 10^{14}$
Average penetration depth, l_{ave} (nm)[a]		360 ± 40
Maximum penetration depth, l_{max} (nm)[a]		830 ± 90
Average kinetic energy of backscattered electrons, E_{bs} (keV)[a]		3.48 ± 0.35
Fraction of backscattered electrons, f_{bs}[a]		0.41 ± 0.04
Average kinetic energy of transmitted electrons, E_{trans} (keV)[a]		0
Fraction of transmitted electrons, f_{trans}[a]		0
Irradiated area, A (cm^2)		1.0 ± 0.1
Dose (eV/molecule)	PH_3	0.8 ± 0.2
	NH_3	0.4 ± 0.1

Note:

[a] Parameters obtained from CASINO software v2.42.

Table S4. Parameters for the vacuum ultraviolet (VUV) light generation used in the present experiments[a].

$2\omega_1 - \omega_2$	Photoionization energy (eV)	10.49 ($3\omega_1$)	9.43	8.80	8.20
	Flux (10^{11} photons s^{-1})	12 ± 1	10 ± 1	10 ± 1	10 ± 1
	Wavelength (nm)	118.222	136.462	140.860	151.200
ω_1	Wavelength (nm)	355	222.566	222.566	249.628
Nd:YAG (YAG A)	Wavelength (nm)	355	355	355	355
Dye laser (DYE A)	Wavelength (nm)	-	445.132	445.132	499.256
Dye		-	Coumarin 450	Coumarin 450	Coumarin 503
ω_2	Wavelength (nm)	-	725	530	715
Nd:YAG (YAG B)	Wavelength (nm)	-	532	355	532
Dye laser (DYE B)	Wavelength (nm)	-	725	530	715
Dye		-	LDS 722	Coumarin 540A	LDS 722
	Nonlinear medium	Xe	Xe	Xe	Xe

Note:

[a] The uncertainty for VUV photon energies is 0.01 eV.

Table S5. Integrated peak areas for all sublimation events.

Precursors		$PH_3 + NH_3$	$PH_3 + {}^{15}NH_3$	$PH_3 + NH_3$	$PH_3 + ND_3$	$PH_3 + ND_3$	$PH_3 + ND_3$
Photon energy (eV)		10.49	10.49	9.43	10.49	10.49	10.49
Molecular formula		NPH_4	$^{15}NPH_4$	NPH_4	NPH_3D	NPH_2D_2	$NPHD_3$
Mass-to-charge ratio (*m/z*)		49	50	49	50	51	52
Sublimation events	125 K	23791 ± 1200	24796 ± 1300	4756 ± 250	4014 ± 200	21586 ± 1100	10045 ± 1000
	132 K	15156 ± 800	16089 ± 800	13707 ± 700	2490 ± 120	14737 ± 750	6310 ± 350
Ratio of 125 K to 132K		1.6 ± 0.1	1.5 ± 0.1	0.4 ± 0.1	1.6 ± 0.1	1.5 ± 0.1	1.6 ± 0.1

Table S6. Computed energies for NPH_4 isomers, corresponding positive ions, and transition states.

	B3LYP/cc-pVTZ + E_{ZPVE} [a] (hartree)	**E_{ZPVE}** [b] (hartree)	**CCSD(T)/CBS** (hartree)	**Relative Energy** (eV)	**Ionization Energy** (eV)
NH_2PH_2	-398.520323	0.043570	-398.026933	0.00	8.60
$NH_2PH_2^+$	-398.211186	0.043428	-397.710843	8.60	-
$NHPH_3$	-398.478365	0.041038	-397.988621	0.97	8.92
$NHPH_3^+$	-398.159975	0.039663	-397.659515	9.89	-
NH_3PH	-398.465332	0.046655	-397.974143	1.52	6.83
NH_3PH^+	-398.219902	0.047348	-397.723980	8.35	-
$HNHPH_2$ (TS1)	-398.401195	0.037305	-397.898055	3.19	-
H_2NHPH (TS2)	-398.432365	0.039639	-397.924600	2.53	-

Notes:

[a] B3LYP/cc-pVTZ energy with zero-point energy correction.

[b] Zero-point vibrational energy at the B3LYP/cc-pVTZ level of theory.

Table S7. Computed Cartesian coordinates (Å) for NPH_4 isomers, corresponding radical cations, and transition states at the B3LYP/cc-pVTZ level of theory.

NH_2PH_2

N	-1.111712	0.042431	-0.080271
P	0.600608	-0.124199	-0.025677
H	-1.540076	0.843052	0.359218
H	-1.602414	-0.803933	0.161871
H	0.951997	1.025124	-0.784132
H	0.963357	0.501721	1.210101

$NHPH_3$

N	0.026606	1.143623	0.000000
P	0.026606	-0.422555	0.000000
H	-0.885816	1.582736	0.000000
H	-0.525988	-1.183988	1.075896
H	-0.525988	-1.183988	-1.075896
H	1.352468	-0.881793	0.000000

NH_3PH

P	-0.7921217	-0.0908793	0.0000000
H	-0.8423248	1.3357677	0.0000000
N	1.1650933	0.0055579	0.0000000
H	1.5104844	-0.9485761	0.0000000
H	1.5291734	0.4690087	-0.8262458
H	1.5291734	0.4690087	0.8262458

$HNHPH_2$ (Transition state)

N	1.1490460	-0.0492760	-0.0691830
P	-0.5069770	0.0394140	-0.0475410
H	1.6069490	-0.5588870	0.6907150
H	-1.2468630	-1.1369590	-0.4372980
H	-1.1185720	0.1995610	1.2250990
H	0.3198130	1.2503000	-0.2811160

NH_2PH_2•+

N	1.066753	0.000022	0.067952
P	-0.575332	0.000025	-0.102572
H	1.603581	-0.852204	-0.057984
H	1.603707	0.852085	-0.058548
H	-1.022166	-1.144100	0.589399
H	-1.022416	1.143690	0.590048

$NHPH_3$•+

N	-0.026631	1.200655	0.000000
P	-0.026631	-0.476493	0.000000

H	0.895064	1.653221	0.000000
H	1.200009	-1.165029	0.000000
H	-0.754593	-0.872693	1.133611
H	-0.754593	-0.872693	-1.133611

NH_3PH•+

P	-0.7698401	-0.0932361	0.0000000
H	-0.8543994	1.3273179	0.0000000
N	1.1290689	0.0035083	0.0000000
H	1.5277000	-0.9372796	0.0000000
H	1.4853588	0.4912166	-0.8256236
H	1.4853588	0.4912166	0.8256236

H_2NHPH (Transition state)

N	-1.2082830	-0.0189010	0.0337610
P	0.7502190	0.0920470	-0.0434280
H	-1.6072340	-0.8172170	-0.4407070
H	-1.6139950	0.8548600	-0.2684600
H	-0.4157290	0.0373840	1.0447020
H	0.8416560	-1.3234340	0.0795540

Table S8. Computed vibrational frequencies (cm^{-1}) and infrared (IR) intensities (km mol^{-1}) for NPH_4 isomers, corresponding radical cations, and transition states at the B3LYP/cc-pVTZ level of theory.

NH_2PH_2			**$NH_2PH_2^{\bullet+}$**		
Normal mode	Frequency	IR Intensity	Normal mode	Frequency	IR Intensity
*v*1	347.87	21.0666	*v*1	410.6071	7.8102
*v*2	505.625	180.3711	*v*2	586.2442	204.0664
*v*3	812.2046	34.6466	*v*3	729.8306	30.5157
*v*4	844.5904	3.6136	*v*4	746.8128	0.7076
*v*5	916.2726	26.3378	*v*5	928.0106	12.5058
*v*6	1082.3691	37.4717	*v*6	1028.0853	31.5831
*v*7	1162.4376	28.8671	*v*7	1045.6572	56.2412
*v*8	1608.6295	17.6392	*v*8	1592.135	56.2412
*v*9	2289.437	145.4656	*v*9	2420.8168	6.3875
*v*10	2367.7668	94.3535	*v*10	2476.7568	4.9036
*v*11	3545.2003	6.8093	*v*11	3493.9604	219.4659
*v*12	3642.5956	23.7305	*v*12	3593.6493	161.8375
$NHPH_3$			**$NHPH_3^{\bullet+}$**		
Normal mode	Frequency	IR Intensity	Normal mode	Frequency	IR Intensity
*v*1	382.0661	104.3082	*v*1	102.9265	106.2699
*v*2	769.0869	9.6992	*v*2	674.9166	53.4213
*v*3	778.8269	84.1786	*v*3	725.4999	19.7666
*v*4	897.7103	82.8175	*v*4	797.2351	19.3111
*v*5	1083.9863	19.2095	*v*5	1008.0525	23.6069
*v*6	1116.0426	11.6375	*v*6	1040.2674	39.4435
*v*7	1131.4108	25.6501	*v*7	1079.9898	1.9719
*v*8	1214.4491	144.3989	*v*8	1086.4531	12.5251
*v*9	2274.1108	170.4879	*v*9	2462.5229	4.6526
*v*10	2312.1243	168.4068	*v*10	2503.1164	15.9136
*v*11	2489.7712	37.5464	*v*11	2503.6183	23.4703
*v*12	3563.9105	15.9966	*v*12	3425.4555	105.2917
NH_3PH			**$NH_3PH^{\bullet+}$**		
Normal mode	Frequency	IR Intensity	Normal mode	Frequency	IR Intensity
*v*1	179.8998	2.4782	*v*1	180.4868	3.9893
*v*2	484.1324	14.0171	*v*2	561.7424	23.7836
*v*3	661.4541	4.0982	*v*3	765.7437	2.3931
*v*4	716.3276	14.675	*v*4	813.2515	16.6955
*v*5	978.2948	38.7621	*v*5	1039.1896	42.0315
*v*6	1280.8821	65.2496	*v*6	1415.5962	99.4336
*v*7	1649.4149	28.6705	*v*7	1640.4934	40.9537
*v*8	1660.5681	33.477	*v*8	1644.2637	46.372
*v*9	2322.3638	144.7158	*v*9	2387.554	16.41
*v*10	3449.2951	7.5069	*v*10	3388.8089	89.2074
*v*11	3533.2786	78.2337	*v*11	3469.8864	123.3789
*v*12	3563.2422	53.8665	*v*12	3483.7403	126.221
$HNHPH_2$ (TS1)			**H_2NHPH (TS2)**		
Normal mode	Frequency	IR Intensity	Normal mode	Frequency	IR Intensity

*v*i	1579.3802i	672.4869	*v*i	1600.2846i	1525.1211
*v*1	627.9111	51.0202	*v*1	297.9648	18.6213
*v*2	698.6944	25.4492	*v*2	512.4325	94.0703
*v*3	809.8643	38.294	*v*3	697.454	64.4965
*v*4	849.6906	46.1526	*v*4	751.5197	5.6969
*v*5	1018.9834	143.8556	*v*5	1009.9825	27.2816
*v*6	1066.2971	30.6975	*v*6	1204.8038	9.8893
*v*7	1203.0071	21.682	*v*7	1519.1763	15.2431
*v*8	2139.6229	153.5091	*v*8	1919.3918	1.8399
*v*9	2212.5882	83.5726	*v*9	2360.3781	93.8395
*v*10	2353.3692	98.0388	*v*10	3493.0622	7.2564
*v*11	3395.0855	0.9136	*v*11	3633.3153	27.8101

Table S9. Comparison of experimental to computed ionization energies (CCSD(T)/CBS//B3LYP/cc-pVTZ + zero-point vibrational energy (ZPVE) corrections) of different nitrogen- and phosphorus- containing compounds with average deviations computed from the error limits. Combined error limits are used to obtain the corrected computed ionization energies.

Compounds	Experimental IE (eV)	Experimental Error Limits (eV)	References	Computed IE (eV)	Computed IE – Experimental IE (max) (eV)	Computed IE – Experimental IE (min) (eV)
Ammonia NH_3	10.070 ± 0.020	10.050 - 10.090	1	10.15	+0.060	+0.100
Phosphine PH_3	9.869 ± 0.002	9.867 - 9.871	1	9.82	–0.051	–0.047
Hydrogen cyanide HCN	13.60 ± 0.01	13.59 - 13.61	1	13.57	–0.04	–0.02
Methinophosphide HCP	10.79 ± 0.01	10.78 - 10.80	2	10.76	–0.04	–0.02
					Average –0.02 ± 0.05	Average 0.00 ± 0.07
					Error Limits –0.07 to +0.03	Error Limits –0.07 to +0.07
					Combined Error Limits ±0.07	

Notes.

Reference 1: Lias (2018)[34]

Reference 2: Frost et al. (1973)[35]

Table S10. Computed Cartesian coordinates (Å), energies (hartree), zero-point vibrational energies (ZPVE) (hartree), vibrational frequencies (cm^{-1}), and infrared (IR) intensities (km mol^{-1}) for ammonia (NH_3), phosphine (PH_3), hydrogen cyanide (HCN), and methinophosphide (HCP) and corresponding radical cations at the CCSD(T)/CBS//B3LYP/cc-pVTZ level of theory.

NH_3				**$NH_3^{\bullet+}$**			
N	0.000000	–0.000000	–0.079087	N	–0.000000	–0.000000	0.000000
H	0.937803	–0.000000	0.306506	H	–1.024664	–0.000000	0.000000
H	–0.468902	0.812162	0.306506	H	0.512332	0.887385	0.000000
H	–0.468902	–0.812162	0.306506	H	0.512332	–0.887385	0.000000
E = –56.5007645				E = –56.1259392			
ZPVE = 0.0342460				ZPVE = 0.0325720			
Frequency	Intensity			Frequency	Intensity		
1067.3138	146.8591			869.9562	232.4392		
1676.8499	16.8512			1529.6011	69.4932		
1676.8499	16.8513			1529.6013	69.4927		
3459.6772	2.3999			3340.0014	0		
3575.8701	0.5378			3514.1724	277.4609		
3575.8703	0.5378			3514.1725	277.4606		
PH_3				**$PH_3^{\bullet+}$**			
P	0.000000	–0.000000	–0.369144	P	–0.000000	–0.000000	–0.170317
H	1.194649	–0.000000	0.402418	H	0.018262	1.353626	–0.545210
H	–0.597325	1.034596	0.402418	H	1.163144	–0.692628	–0.545210
H	–0.597325	–1.034596	0.402418	H	–1.181405	–0.660998	–0.545210
E = –342.7140405				E = –342.3528353			
ZPVE = 0.0238100				ZPVE = 0.0234560			
Frequency	Intensity			Frequency	Intensity		
1020.6955	19.9072			735.6199	2.8049		
1138.3099	11.0143			1039.5932	6.6989		
1138.3099	11.0144			1039.5936	6.6982		
2379.1784	34.9882			2442.4331	13.6025		

2387.4073	67.7605
2387.4078	67.7536

HCN			
C	0.000000	0.000000	–0.502032
N	0.000000	0.000000	0.655879
H	0.000000	0.000000	–1.578957

E = –93.3125436
ZPVE = 0.0164250

Frequency	Intensity
771.8606	34.1125
771.8606	34.1125
2200.5474	2.0382
3465.485	63.2406

HCP			
C	0.000000	0.000000	–1.007293
P	0.000000	0.000000	0.542255
H	0.000000	0.000000	–2.090069

E = –379.5170519
ZPVE = 0.0138850

Frequency	Intensity
709.0494	66.5025
709.0494	66.5025
1329.7237	0.1463
3346.9931	15.3657

2519.443	51.1202
2519.4441	51.1287

$HCN^{\bullet+}$			
C	0.000000	0.000000	–0.530335
N	0.000000	0.000000	0.688215
H	0.000000	0.000000	–1.635498

E = –92.8117700
ZPVE = 0.0144460

Frequency	Intensity
503.9549	11.4409
741.9941	44.7645
1905.8395	16.5557
3189.4461	285.7971

$HCP^{\bullet+}$			
C	0.000000	0.000000	–1.049586
P	0.000000	0.000000	0.562870
H	0.000000	0.000000	–2.145534

E = –379.1208937
ZPVE = 0.0130650

Frequency	Intensity
642.0067	14.0614
675.3419	83.28
1181.4996	1.5103
3235.9601	176.6135

Table S11. Computed Cartesian coordinates (Å), energies (hartree), zero-point vibrational energies (ZPVE) (hartree), vibrational frequencies (cm^{-1}), and infrared (IR) intensities (km mol^{-1}) for the transition state of intermolecular H-transfer between two phosphine imide ($HNPH_3$, **1**) molecules.

Transition state (2 $HNPH_3$ → 2 H_2NPH_2) (*C*s)

N	–1.103256	–1.211343	0.000000
P	–1.721962	0.284035	0.000000
H	–1.729118	–2.006867	0.000000
H	–2.609761	0.591450	–1.072386
H	–2.609761	0.591450	1.072386
H	–0.434014	1.124769	0.000000
N	1.120144	1.220745	0.000000
P	1.714929	–0.287758	0.000000
H	1.774507	1.994229	0.000000
H	2.612425	–0.599376	–1.067562
H	2.612425	–0.599376	1.067562
H	0.360404	–1.117310	0.000000

E = –797.0309476
E[CCSD(T)/CBS] = –795.9534542
ZPVE = 48.8876 kcal mol–1
ν_i = 1267.3 cm–1

Frequency	Intensity
–1267.328	279.1082
88.2856	2418.2115
92.2544	20.8167
174.9409	1.5006
203.7356	23.65
234.3484	29.7009
424.528	9.1398
443.6295	120.372
469.8318	72.4186
680.2522	1798.1895
781.3588	0.2313
802.8763	15.8852
856.16	0.2448
901.0613	73.1429
954.1316	6.3444
1011.0857	1172.2736
1051.7761	14.6685
1076.5199	22.3075
1092.8477	0.0099

1135.67	2.1412
1185.4681	3.3951
1189.4863	92.2711
1497.2238	256.9305
1558.7658	512.2684
2286.3961	132.2571
2299.1268	231.6814
2312.5298	138.6859
2323.137	113.8021
3527.4452	1.7321
3542.5036	3.5992

References

1. B. M. Jones and R. I. Kaiser, *J. Phys. Chem. Lett.*, 2013, **4**, 1965-1971.
2. L. Zhou, S. Maity, M. Abplanalp, A. Turner and R. I. Kaiser, *Astrophys. J.*, 2014, **790**, 38.
3. A. M. Turner, M. J. Abplanalp, S. Y. Chen, Y. T. Chen, A. H. Chang and R. I. Kaiser, *Phys. Chem. Chem. Phys.*, 2015, **17**, 27281-27291.
4. A. Dawes, R. J. Mukerji, M. P. Davis, P. D. Holtom, S. M. Webb, B. Sivaraman, S. V. Hoffmann, D. A. Shaw and N. J. Mason, *J. Chem. Phys.*, 2007, **126**, 244711.
5. M. Satorre, J. Leliwa-Kopystynski, C. Santonja and R. Luna, *Icarus*, 2013, **225**, 703-708.
6. B. Wood and J. Roux, *J. Opt. Soc. Am.*, 1982, **72**, 720-728.
7. T. Shimanouchi, *J. Phys. Chem. Ref. Data*, 1977, **6**, 993-1102.
8. J. H. Teles, G. Maier, B. Andes Hess Jr and L. J. Schaad, *Chem. Ber.*, 1989, **122**, 749-752.
9. G. Socrates, *Infrared and Raman Characteristic Group Frequencies*, John Wiley & Sons, Ltd., New York, 3rd edn., 2004.
10. J. S. Holt, D. Sadoskas and C. J. Pursell, *J. Chem. Phys.*, 2004, **120**, 7153-7157.
11. W. Zheng, D. Jewitt, Y. Osamura and R. I. Kaiser, *Astrophys. J.*, 2008, **674**, 1242.
12. J. Hollenberg and D. A. Dows, *J. Chem. Phys.*, 1961, **34**, 1061-1062.
13. B. Teolis, M. Loeffler, U. Raut, M. Famá and R. Baragiola, *Icarus*, 2007, **190**, 274-279.
14. K. I. Öberg, R. T. Garrod, E. F. Van Dishoeck and H. Linnartz, *Astron. Astrophys.*, 2009, **504**, 891-913.
15. M. Bouilloud, N. Fray, Y. Benilan, H. Cottin, M. C. Gazeau and A. Jolly, *Mon. Not. Roy. Astron. Soc.*, 2015, **451**, 2145-2160.
16. S. A. Sandford and L. J. Allamandola, *Astrophys. J.*, 1993, **417**, 815-825.
17. D. Drouin, A. R. Couture, D. Joly, X. Tastet, V. Aimez and R. Gauvin, *Scanning*, 2007, **29**, 92-101.
18. Gaussian 09, Revision D.01, M. J. Frisch, G. W. Trucks, H. B. Schlegel, G. E. Scuseria, M. A. Robb, J. R. Cheeseman, G. Scalmani, V. Barone, B. Mennucci, G. A. Petersson, H. Nakatsuji, M. Caricato, X. Li, H. P. Hratchian, A. F. Izmaylov, J. Bloino, G. Zheng, J. L. Sonnenberg, M. Hada, M. Ehara, K. Toyota, R. Fukuda, J. Hasegawa, M. Ishida, T. Nakajima, Y. Honda, O. Kitao, H. Nakai, T. Vreven, J. A. Montgomery, Jr., J. E. Peralta, F. Ogliaro, M. Bearpark, J. J. Heyd, E. Brothers, K. N. Kudin, V. N. Staroverov, T. Keith, R. Kobayashi, J. Normand, K. Raghavachari, A. Rendell, J. C. Burant, S. S. Iyengar, J. Tomasi,

M. Cossi, N. Rega, J. M. Millam, M. Klene, J. E. Knox, J. B. Cross, V. Bakken, C. Adamo, J. Jaramillo, R. Gomperts, R. E. Stratmann, O. Yazyev, A. J. Austin, R. Cammi, C. Pomelli, J. W. Ochterski, R. L. Martin, K. Morokuma, V. G. Zakrzewski, G. A. Voth, P. Salvador, J. J. Dannenberg, S. Dapprich, A. D. Daniels, O. Farkas, J. B. Foresman, J. V. Ortiz, J. Cioslowski, and D. J. Fox, Gaussian, Inc., Wallingford CT, **2013**.

19. Gaussian 16, Revision A.03; Frisch, M. J.; Trucks, G. W.; Schlegel, H. B.; Scuseria, G. E.; Robb, M. A.; Cheeseman, J. R.; Scalmani, G.; Barone, V.; Petersson, G. A.; Nakatsuji, H.; Li, X.; Caricato, M.; Marenich, A. V.; Bloino, J.; Janesko, B. G.; Gomperts, R.; Mennucci, B.; Hratchian, H. P.; Ortiz, J. V.; Izmaylov, A. F.; Sonnenberg, J. L.; Williams-Young, D.; Ding, F.; Lipparini, F.; Egidi, F.; Goings, J.; Peng, B.; Petrone, A.; Henderson, T.; Ranasinghe, D.; Zakrzewski, V. G.; Gao, J.; Rega, N.; Zheng, G.; Liang, W.; Hada, M.; Ehara, M.; Toyota, K.; Fukuda, R.; Hasegawa, J.; Ishida, M.; Nakajima, T.; Honda, Y.; Kitao, O.; Nakai, H.; Vreven, T.; Throssell, K.; Montgomery, J. A., Jr.; Peralta, J. E.; Ogliaro, F.; Bearpark, M. J.; Heyd, J. J.; Brothers, E. N.; Kudin, K. N.; Staroverov, V. N.; Keith, T. A.; Kobayashi, R.; Normand, J.; Raghavachari, K.; Rendell, A. P.; Burant, J. C.; Iyengar, S. S.; Tomasi, J.; Cossi, M.; Millam, J. M.; Klene, M.; Adamo, C.; Cammi, R.; Ochterski, J. W.; Martin, R. L.; Morokuma, K.; Farkas, O.; Foresman, J. B.; Fox, D. J., Gaussian Inc., Wallingford CT 2016.
20. A. D. Becke, *Physical Review A*, 1988, **38**, 3098-3100.
21. A. D. Becke, *J. Chem. Phys.*, 1993, **98**, 5648-5652.
22. C. Lee, W. Yang and R. G. Parr, *Physical Review B*, 1988, **37**, 785-789.
23. J. Dunning, Thom H., *J. Chem. Phys.*, 1989, **90**, 1007-1023.
24. J. Čížek, *J. Chem. Phys.*, 1966, **45**, 4256-4266.
25. R. J. Bartlett, J. D. Watts, S. A. Kucharski and J. Noga, *Chem. Phys. Lett.*, 1990, **165**, 513-522.
26. K. Raghavachari, *Annu. Rev. Phys. Chem.*, 1991, **42**, 615-642.
27. J. F. Stanton, *Chem. Phys. Lett.*, 1997, **281**, 130-134.
28. K. A. Peterson, D. E. Woon and T. H. Dunning, *J. Chem. Phys.*, 1994, **100**, 7410-7415.
29. T. J. Lee and P. R. Taylor, *Int. J. Quantum. Chem.*, 1989, **36**, 199-207.
30. C. Zhu, R. Frigge, A. Bergantini, R. C. Fortenberry and R. I. Kaiser, *Astrophys. J.*, 2019, **881**, 156.

31. E. D. Glendening, J. K. Badenhoop, A. E. Reed, J. E. Carpenter, J. A. Bohmann, C. M. Morales, C. R. Landis and F. Weinhold, NBO, version 6.0; Theoretical Chemistry Institute, University of Wisconsin: Madison, WI, **2013**.
32. H. Sabzyan and Z. Kalantar, *J. Mol. Struct.: THEOCHEM*, 2003, **663**, 149-157.
33. W. C. Lu, C. B. Liu and C. C. Sun, *J. Phys. Chem. A*, 1999, **103**, 1078-1083.
34. Sharon G. Lias, "Ionization Energy Evaluation" in NIST Chemistry WebBook, NIST Standard Reference Database Number 69, Eds. P.J. Linstrom and W.G. Mallard, National Institute of Standards and Technology, Gaithersburg MD, 20899, https://doi.org/10.18434/T4D303, 2018.
35. D. Frost, S. Lee and C. McDowell, *Chem. Phys. Lett.*, 1973, **23**, 472-475.